[Short title + Author Name - P&H title] 18 (2025) 106034

Contents lists available at ScienceDirect

Arabian Journal of Chemistry

journal homepage: www.ksu.edu.sa

Ultra-fine carbon decorated TiO_2/C/g-C_3N_4 hybrid for strong physical adsorption and efficient photodegradation of pollutants

Azim Khan [a,b,1], Ruhumuriza Jonathan [a,b,1], Shafiq Ur Rehman [a,b,1], Muhammad Shoaib [a,b], Feng Cao [c], Sajjad Ali [e], Mohamed Bououdina [e], Pir Muhammad Ismail [e], Junwei Wang [a,*], Hazem Abu-Farsakh [e], Yifan Liu [a], Xian Jian [a,b,d,*]

[a] Yangtze Delta Region Institute (Huzhou), University of Electronic Science and Technology of China, Huzhou 313001, China
[b] School of Materials and Energy, University of Electronic Science and Technology of China, Chengdu 611731, China
[c] Department of Engineering Technology, Huzhou College, Huzhou 313000, China
[d] Zhejiang Humo Polishing Grinder Manufacture Co. Ltd., Huzhou 313012, China
[e] Energy, Water, and Environment Lab, College of Humanities and Sciences, Prince Sultan University, Riyadh 11586, Saudi Arabia

ARTICLE INFO

Keywords:
TiO_2/C/g-C_3N_4 hybrid
Photocatalysis
Charge separation efficiency
Formaldehyde
Organic pollutant degradation

ABSTRACT

Enhancement in the visible light absorption and efficient interfacial charge transfer is crucial for optimizing photocatalytic efficiency in the degradation of pollutants such as methyl orange (MO) and formaldehyde. This study focuses on the properties of a TiO_2/C/g-C_3N_4 hybrid efficient photocatalyst, which is developed using an air calcination method to deposit graphitic nitride (g-C_3N_4) onto a carbon-modified TiO_2 surface. The characterization techniques, including high-resolution transmission electron Microscopy (HRTEM), X-ray diffraction (XRD), Raman spectroscopy, thermogravimetric analysis (TGA), Fourier-transform infrared spectroscopy (FTIR), and X-ray photoelectron spectroscopy (XPS), were used to provide a comprehensive understanding of the material's structural, morphological, thermal, and chemical properties. This hybrid catalyst is specifically engineered for the efficient decomposition of methyl orange (MO) and formaldehyde, demonstrating a significant increase in photocatalytic activity. The TiO_2/C/g-C_3N_4 photocatalyst also exhibits an enhanced specific surface area of 181.2 m^2/g, which facilitates increased physical adsorption and photo-catalytic active sites. Experimental results confirm that this catalyst effectively adsorbs MO physically even in the dark without degradation. Combining physical and photo-catalytic functions, this catalyst degrades 94 % of MO within 180 min with the initial concentration 0.2 mol/L of MO, and achieves almost 100 % decolorization of MO under visible light irradiation. Notably, the catalyst retains its high activity after 4 cycles of MO degradation, underscoring its durability and consistent performance. Additionally, the hybrid catalyst features a staggered type-II energy level configuration, which effectively enhances charge separation and boosts photocatalytic efficacy. The incorporation of an ultrafine carbon layer further augments electron mobility towards the surface, crucial for effective catalytic reactions. This study paves the way for future development of highly efficient photocatalytic materials for environmental purification.

1. Introduction

Recently, photocatalysis has been attracted tremendous interest due to their wide spread applications. This interest arises from an increasing understanding of their real-world benefits in fields such as renewable energy, environmental remediation, and water purification. Using solar energy, photocatalysis shows great potential in producing chemical fuels and cleaning the environment by decontaminating various pollutants. These catalysts have attracted attention due to their efficacy in degrading complex organic pollutants, presenting promising prospects for diverse practical applications (Dalanta et al., 2022; Shi et al., 2023; Wang et al., 2010; Lu et al., 2010; Wang et al., 2019; Yan et al., 2023; Li

* Corresponding authors at: Yangtze Delta Region Institute (Huzhou), University of Electronic Science and Technology of China, Huzhou 313001, China (Xian Jian).
E-mail addresses: wjw@csj.uestc.edu.cn (J. Wang), jianxian@uestc.edu.cn (X. Jian).
[1] These authors are equally contributed.

https://doi.org/10.1016/j.arabjc.2024.106034
Received 6 July 2024; Accepted 20 October 2024
Available online 24 October 2024

et al., 2022; Xin et al., 2021; Yin et al., 2022; Osterloh, 2013; Wang and Wang, 2022). Since the pioneering report by Fujishima and Honda in 1979 (Cao et al., 2013; Inoue et al., 1979) various photocatalysts have been developed, such as, TiO_2, g-C_3N_4, WO_3, SiC, ZnO, and ZnS for various photocatalytic application. Due to outstanding properties, TiO_2 remains the most widely studied photocatalyst (Liyanaarachchi et al., 2023; Bashir et al., 2022; Wang and Wang, 2022; Bao et al., 2023; Ismael, 2020; Sun et al., 2020; Wu et al., 2023; Han et al., 2023; Cui and Sun, 2006). The g-C_3N_4 (graphitic carbon nitride) has promising characteristics, including 2.7 eV band gap, non-toxicity, affordability, and potential for industrial and combustion applications (Wudil et al., 2023; Ismael, 2020; Sun et al., 2020; Que et al., 2021; Wang et al., 2023; Guo et al., 2021). It also has exciting electrical and electrochemical properties which make it, a candidate material for applications into optoelectronic, photonic, photocatalysis, electrocatalysis, batteries and for degradation of organic pollutants (Nguyen et al., 2020; Ismael, 2020; Que et al., 2021; Wang et al., 2023). According to measurements with normal hydrogen electrode (NHE), it has been determined that the potential difference between the conduction and valence bands in graphitic carbon nitride is 1.3 eV and 1.4 eV. These values are particularly favorable for facilitating efficient water splitting (Ismael, 2020; Wang et al., 2023). However, the current visible light photocatalytic activity of pure g-C_3N_4 is still low, mainly due to the unoptimized electronic structure of g-C_3N_4 material, which leads to a high rate of photocarrier recombination and a large bandgap width (~2.8 eV), preventing the effective utilization of sunlight. Various approaches have been developed to overcome this challenge such as element doping, modified with other composites semiconducting materials. These strategies in photocatalysts increase the diffusion length of photogenerated carriers that prolong the lifetime of charges, inhibiting the internal recombination rate of charges. In addition, element doping favors the photons with small energy excited electrons (e^-) and holes (h^+) captured at doping levels, which improves the utilization rate of photons and optimize the visible light absorption of photocatalysts (Djurišić et al., 2014). One promising research direction is the hybrid formation of g-C_3N_4 with other semiconductor composites, which facilitate the negative charge flow and reducing their recombination with positive charges (Sun et al., 2020; Cui and Sun, 2006; Djurišić et al., 2014; Xin et al., 2021; Yin et al., 2022; Xu et al., 2024). TiO_2 has been used widely to construct hybrid, effectively separating and transferring photogenerated carriers (Shaban, 2019; Xin et al., 2021; Yin et al., 2022; Jonathan et al., 2023; Chen et al., 2023; Guo et al., 2020). Jin Luo et al. reported the development of two innovative Z-scheme photocatalysts: a $LaMnO_3$/g-C_3N_4 hybrid, constructed for efficient visible-light-driven degradation of tetracycline (TC), and an AgI/$Zn_3V_2O_8$ hybrid, where AgI nanoparticles were immobilized on flower-like $Zn_3V_2O_8$ nanosheets via a simple precipitation method. Both designs utilize the Z-scheme mechanism to enhance photocatalytic performance (Luo et al., 2019; Luo et al., 2021). Similarly, Lin et al. synthesized a CdS/ZnS core/shell structure,where zinc vacancies transformed the type-I heterojunction into a Z-scheme hybrid, enabling the ZnS shell to effectively capture photogenerated holes from the CdS core (Lin et al., 2020). TiO_2 shows potential for forming a hybrid structure with g-C_3N_4. However, its small surface area has limited its photocatalytic efficiency. Co-doping in TiO_2/C_3N_4 has demonstrated significant enhancement in catalytic performance attributed to the availability of more active sites (Huang et al., 2021).

Jiao et al, developed an ultrasmall (~5 nm) visible-light-responsive TiO_2/C photocatalyst with a hybrid structure via chemical vapor deposition. The monolayer carbon shell enhances charge separation, stabilizes Ti^{3+}, and narrows the bandgap (2.83 eV), leading to superior photocatalytic performance for water oxidation, dye degradation, and hydrogen evolution. This design provides a promising approach for industrial applications requiring stable, visible-light-responsive photocatalysts (Jiao et al., 2022). In comparison, the TiO_2/C/g-C_3N_4 photocatalyst, developed via a facile heat-treatment method, incorporates an ultrafine carbon layer to enhance electron mobility, improving catalytic performance through both physical adsorption and chemical degradation. Both designs focus on enhancing photocatalytic efficiency, with one emphasizing structural stability and bandgap tuning, and the other excelling in adsorption capacity and recyclability. The hybrid of TiO_2 with C_3N_4 facilitates to separate charges at junction interface. This configuration control the hole recombination with electron because of very low valence band edge potential of TiO_2. But electrons in C_3N_4 still do not have enough potentials to trigger the chemical reactions with the organic pollutant and to reduce it. Before, the reaction initiates the electrons recombine with holes in the host material and decomposes the material. Therefore, an external facilitator is needed to boost up the electron transfer mechanisms in the staggered band alignment and hence increase the degradation of organic pollutant. Based on a detailed literature survey, the TiO_2/C/g-C_3N_4 hybrid photocatalyst was first developed through a facile heat-treatment process, incorporating an ultrafine carbon layer to enhance electron mobility for more efficient catalytic reactions. Secondly, this facile heat-treatment method in air is valuable for the large-scale preparation of photocatalysts, up to 1 kg, employing an air calcination process to deposit graphitic nitride (g-C_3N_4) onto a carbon-modified TiO_2 surface. While many researchers have studied how photocatalyst performance can be enhanced by either physical adsorption or chemical degradation of pollutants. Thirdly, the innovative aspect of the present work lies in coupling both physical adsorption and chemical degradation to improve photocatalytic performance.

In this study, we have applied a straightforward air calcination technique to fabricate a unique hybrid structure with a carbon (C) layer acting as a separator. This design not only facilitates efficient electron transfer but also hinders recombination with holes. These advancements significantly elevate the quantum efficiency, thereby augmenting the degradation of both atmospheric and organic pollutants. This work is really important for cleaning up the environment and can be used in many different industries. This study introduces a photocatalyst called TiO_2/C/g-C_3N_4, which is really effective in decomposing methyl orange and formaldehyde. The surface engineering of air calcination process to design the ultrafine carbon layer to bridge TiO_2 and g-C_3N_4 with strong physical absorption as well as enhanced photocatalytic performance.

2. Experimental section

2.1. Materials and chemical

Urea (H_2NCONH_2) ≥ 99.5 %), Formaldehyde solution (CH_2O, 37 wt % in H_2O) and Methyl Orange ($C_{14}H_{14}N_3NaO_3S$) were purchased from China based companies, Shanghai Titan Scientific Co.ltd and Shanghai Aladdin Biochemical Technology Co. ltd.

2.2. Preparation of TiO_2/C/g-C_3N_4 photocatalyst

The TiO_2/C_7H_8O powder was prepared using the sol–gel method to regulate the hydrolysis rate of titanium tetrachloride ($TiCl_4$). A gradual dissolution of $TiCl_4$ (6.25 mL) was performed in one liter of benzyl alcohol (C_7H_8O), with the solution stirred at 50 °C for five days. The resulting solid product was centrifuged and washed multiple times with alcohol to eliminate a significant portion of the adsorbed C_7H_8O. The product was then heated at 60 °C for 24 h, yielding white TiO_2 powder. Similarly, we got the g-C_3N_4 by gradually added (10 g) of urea into deionized water of 50 ml. The solution was stirred for one hour in a water bath at 60 °C, and then the TiO_2/C composite was prepared by chemical vapor deposition (CVD) method. The g-C_3N_4 was mixed with TiO_2/C and 50 ml of deionized water, then sonicated and stirred for 20 min at 60 °C. The following molar ratios of urea to TiO_2 were used to form the hybrid: 1:1, 2.5:1, and 5:1. The solution was heated to 60 °C until all the solvent evaporated, leaving the Urea/TiO_2 precursor. This precursor was then converted to powder form through precipitation and calcination at 500 °C for two hours in an aerobic environment. The

carbonized particles were washed through distilled water and ethanol, then heated at 60 °C to obtain the hybrid of (TiO_2/C/g-C_3N_4) sample. Considering different ratios TiO_2 andg-C_3N_4 several hybrids were prepared referred to as, (TiO_2/C/g-C_3N_4-1), (TiO_2/C/g-C_3N_4-2), and (TiO_2/C/g-C_3N_4-3). We study the MO and HCHO degradation performance in visible light using light emitting diode (LED), and temperature control system was set at the room temperature of 25 °C.

2.3. Characterization

The phase structures of the specimens were characterized by X-ray diffraction (XRD) using a RIGAKU Miniflex X600 instrument. Morphological and crystallographic analyses were conducted using high-resolution transmission electron microscopy (HRTEM) at an acceleration voltage of 200 kV. The surface chemical compositions of Ti, O, and C in various samples were determined through X-ray photoelectron spectroscopy (XPS), using a Thermo-Scientific instrument with an Al Kα X-ray source. The binding energy was calibrated against the contaminant carbon at 284.8 eV. Infrared spectroscopy measurements were performed using a BRUKER-VERTEX 70 spectrometer, covering a spectral range from 4000 to 400 cm^{-1}. Raman spectra were acquired using a LabRam HR 800 instrument to validate the fundamental nature of TiO_2. UV–vis absorbance spectra were obtained with a UV–visible spectrophotometer (UV2600) in the range of 200–800 nm. Thermogravimetric analysis (TGA) was conducted under a nitrogen (N_2) atmosphere at a heating rate of 30 °C/min, spanning from room temperature to 800 °C.

2.4. Photocatalytic degradation of MO and formaldehyde

Initially, the prepared hybrid catalysts were examined by measuring their photocatalytic activity using methyl orange (MO) as the target compound for degradation. Typically, 50 mL of MO solution was diluted with 2.5 mg of photocatalyst (0.2 mol/L). When the suspension was stirred and mixed for 10 min, before exposing to 200 W LED lamp. During a specified time interval, the solution was extracted and subsequently subjected to centrifugation. The resulting solution was analyzed in a visible to ultra violet light illumination at wavelength 446 nm to measure the MO degradation in the supernatant. Furthermore, a specially designed device was used to study the photocatalytic degradation of formaldehyde (HCHO). A 10 mL and 30 gL^{-1} catalyst suspension were sprayed on a piece of cotton cloth, and then 1 mL, 37 wt% HCHO solution sprayed on the surface of the cloth. The chamber is equipped with a fan, which can evenly diffuse the vapors of HCHO vapor. Then the cloth was irradiated by four 5 W LEDs, the volatilization amount of HCHO in the transparent chamber was monitored and recorded by the sensors (HCHO). We have used the LED to study the catalytic process of MO and HCHO degradation and the temperature control system was adjusted to room temperature (25 °C).

3. Results and discussion

The conventional approach to photocatalytic degradation of pollutants primarily involves structural and energy level modulation to extend

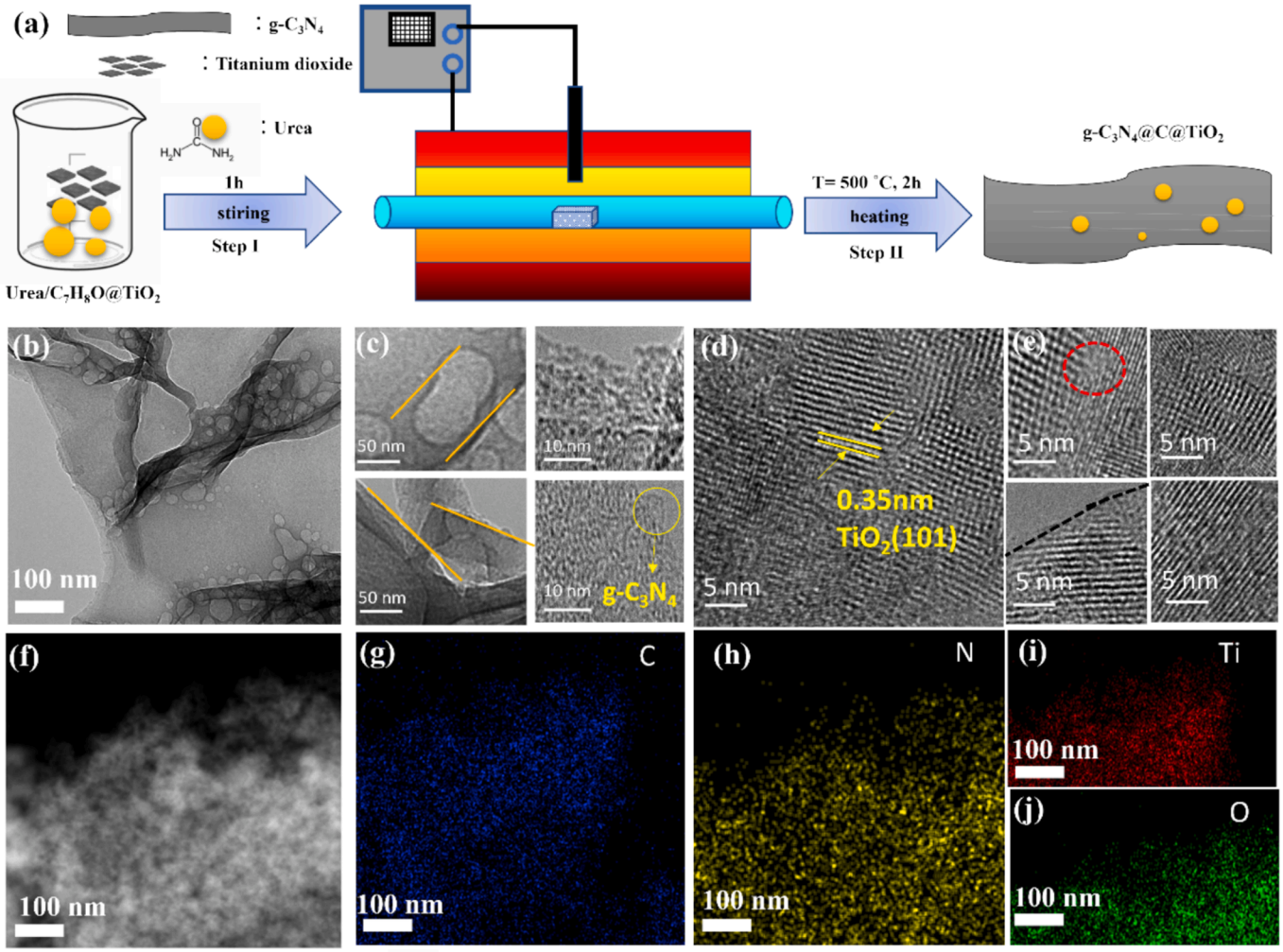

Fig. 1. (a) Graphical representation of the TiO_2/C/g-C_3N_4 hybrid preparation by air calcination method at 500 °C. (b–c) TEM results of g-C_3N_4 and (d–e) TiO_2/C/g-C_3N_4 (f–j) Mapping of elements; C (g), N (h), Ti (i) and O (j) elements of TiO_2/C/g-C_3N_4.

catalytic responsiveness from ultraviolet (UV) to visible light spectra, thereby facilitating the decomposition of pollutants in air or water. In this study, a novel strategy is proposed, integrating physical adsorption and photocatalysis in a hybrid framework. This 3D carbon layer bridging structures effectively exert the physical adsorption function of carbon materials, and also regulate the energy level structure of the materials, achieving a dual functional combination of physical adsorption and photocatalysis. The hybrid photocatalyst, denoted as $TiO_2/C/g\text{-}C_3N_4$, is synthesized through a straightforward heating process under normal atmospheric pressure, as illustrated in Fig. 1a. Urea mixed with TiO_2/C_7H_8O was stirred for 1 h then heated in the furnace inset covered crucible at 500 °C for 2 h, yielding the $TiO_2/C/g\text{-}C_3N_4$ hybrid with desired photocatalytic properties. Moreover, characterization of the morphologies of the graphitized carbon nitride, TiO_2, and ($TiO_2/C/g\text{-}C_3N_4$) samples is performed using high-resolution transmission electron microscopy (HRTEM), as depicted in Fig. 1(b–e). Fig. 1c clearly shows that $g\text{-}C_3N_4$ has a layered structure, indicated by the yellow lines. The HRTEM images of $g\text{-}C_3N_4$ reveal an amorphous layer structure, while the observed lattice fringe of 0.35 nm in the $TiO_2/C/g\text{-}C_3N_4$ hybrid corresponds to the (1 0 1) planes of TiO_2 (Chen et al., 2017). During the CVD process, the residual organic material underwent decomposition into carbon (C) atoms that are highly reactive, which were doped directly onto TiO_2 surface. The surface of $TiO_2/C/g\text{-}C_3N_4$ displays disordered carbon layers indicated by black dotted line, and potential defects indicated by red circle as shown in Fig. 1e. Elemental mapping for C, N, Ti and O elements in the $TiO_2/C/g\text{-}C_3N_4$ hybrid formation is presented in Fig. 1(f-j), respectively.

The crystal phase of $TiO_2/C/g\text{-}C_3N_4$ hybrid photocatalyst was identified using XRD (X-ray diffraction) technique and the results are given in Fig. 2a. All diffraction peaks of TiO_2/C_7H_8O and $TiO_2/C/g\text{-}C_3N_4$ correspond to the TiO_2 anatase phases, which mean that the TiO_2/C_7H_8O and $TiO_2/C/g\text{-}C_3N_4$ hybrids belong to the anatase phases of TiO_2. Additionally, the spectra (XRD) of TiO_2/C_7H_8O and TiO_2/C hybrids exhibits four well-defined diffraction peaks at the lattice planes of (1 0 1), (004), (200), and (105) respectively, in agreement with previous investigations (Zhang et al., 2023; Xiao et al., 2023). This indicates that the crystal structure of TiO_2/C_7H_8O remains unchanged following high-temperature calcination and the addition of carbon capsules. Actually, the carbon capsules act as a protective barrier during high-temperature calcination, preventing excessive grain growth and limiting agglomeration of TiO_2 nanoparticles, thereby preserving a well-defined crystalline structure. Additionally, they stabilize the photo-catalytically active anatase phase by buffering against phase transitions to rutile at elevated temperatures, ensuring the catalyst retains its optimal photocatalytic performance. Moreover, the observed peaks at (1 0 0) and (004) align with those characteristics of $g\text{-}C_3N_4$, consistent with findings in existing literature (Chen et al., 2023).

The structure and molecular composition of $TiO_2/C/g\text{-}C_3N_4$ hybrids were analyzed using the Raman technique, which revealed that the TiO_2/C_7H_8O and $TiO_2/C/g\text{-}C_3N_4$ hybrids have peaks at 152, 392, 515, and 631 cm^{-1} as given in Fig. 2b. These peaks correspond to the four basic modes of titanium dioxide (E_g, $B1_g$, $A1_g$, and Eg), indicating that the anatase phase of TiO_2 is not affected by the in-situ addition of carbon capsule in $TiO_2/C/g\text{-}C_3N_4$ (Cui, 2006; Yao et al., 2021).

Thermogravimetric analysis (TGA) was performed under open platform conditions, encompassing from room temperature to 800 °C with a heating rate of 30 °C/min, aimed at elucidating the thermostability of the hybrid. The TGA results (Fig. 2c) illustrate notable weight loss

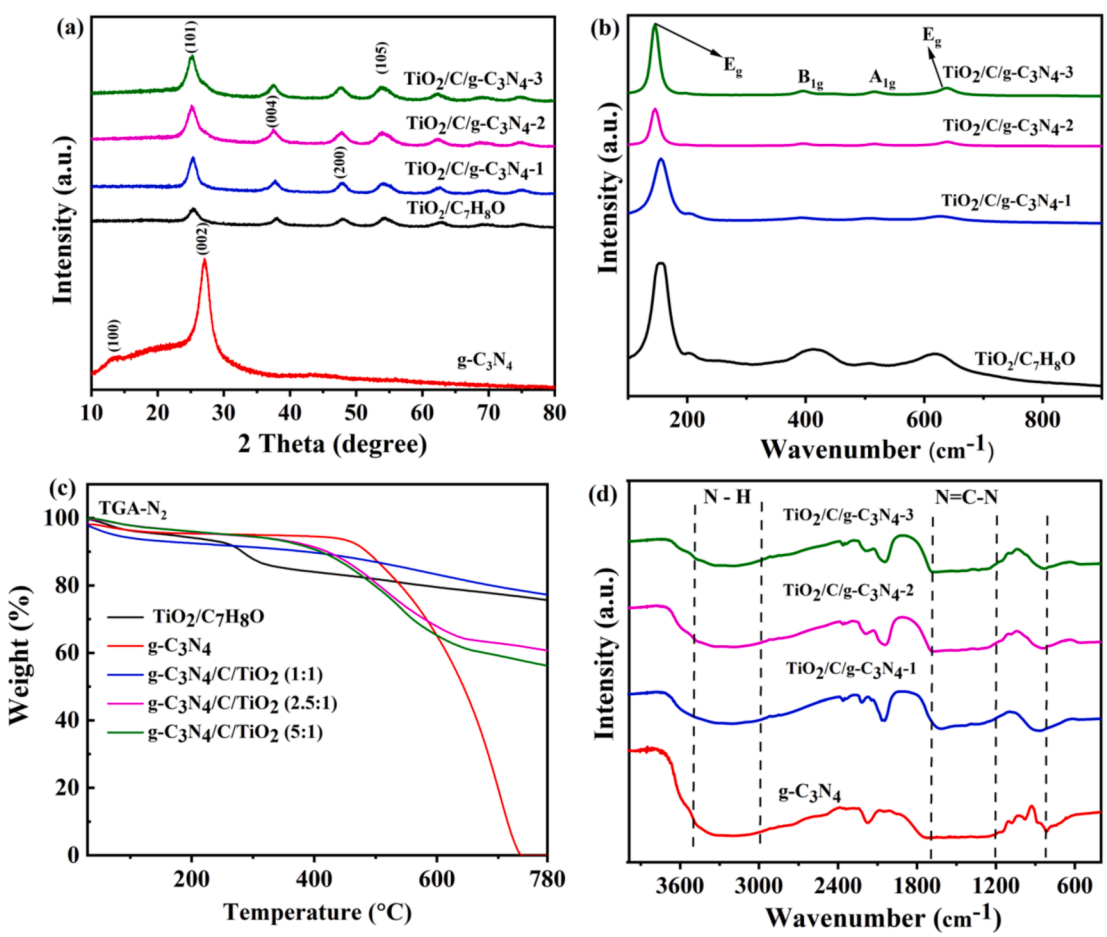

Fig. 2. (a) XRD patterns, (b) Raman spectra, (c) TGA, and (d) FTIR of TiO_2/C_7H_8O, $g\text{-}C_3N_4$, $TiO_2/C/g\text{-}C_3N_4$-1, $TiO_2/C/g\text{-}C_3N_4$-2 and $TiO_2/C/g\text{-}C_3N_4$-3, respectively.

phases occurring primarily between ambient temperature and 200 °C. This phenomenon is attributed to the dissociation of adsorbed and intercalated water molecules. Notably, g-C_3N_4 undergoes fast weight loss within the temperature interval of 400 to 780 °C, resulting in substantial weight reduction during this range. At 750 °C, pure g-C_3N_4 experiences complete weight loss, indicative of its compositional transformation during decomposition. The second stage of weight loss reveals that the g-C_3N_4 quantity present in the composites based on their weight. The measured quantity of g-C_3N_4 in the photocatalysts were determined as 93.6 %, 88.8 %, and 77.7 % by weight for samples TiO_2/C/g-C_3N_4-1, TiO_2/C/g-C_3N_4-2, and TiO_2/C/g-C_3N_4-3, respectively. Noteworthy is the lower initial weight loss temperature observed in the TiO_2/C/g-C_3N_4-1 sample, attributed to the elevated ratio of TiO_2. This higher TiO_2 ratio facilitates catalytic oxidation of g-C_3N_4, even at temperatures below 600 °C.

FTIR spectroscopy was employed to further analyze the components of prepared catalysts. As depicted in Fig. 2d, both g-C_3N_4 and TiO_2/C/g-C_3N_4-(1, 2,3) hybrids display typical peaks (absorption) for g-C_3N_4. The sharp peak of g-C_3N_4, located at approximately 800 cm^{-1} corresponds to the inherent vibrational modes, specifically the breathing motions of s-

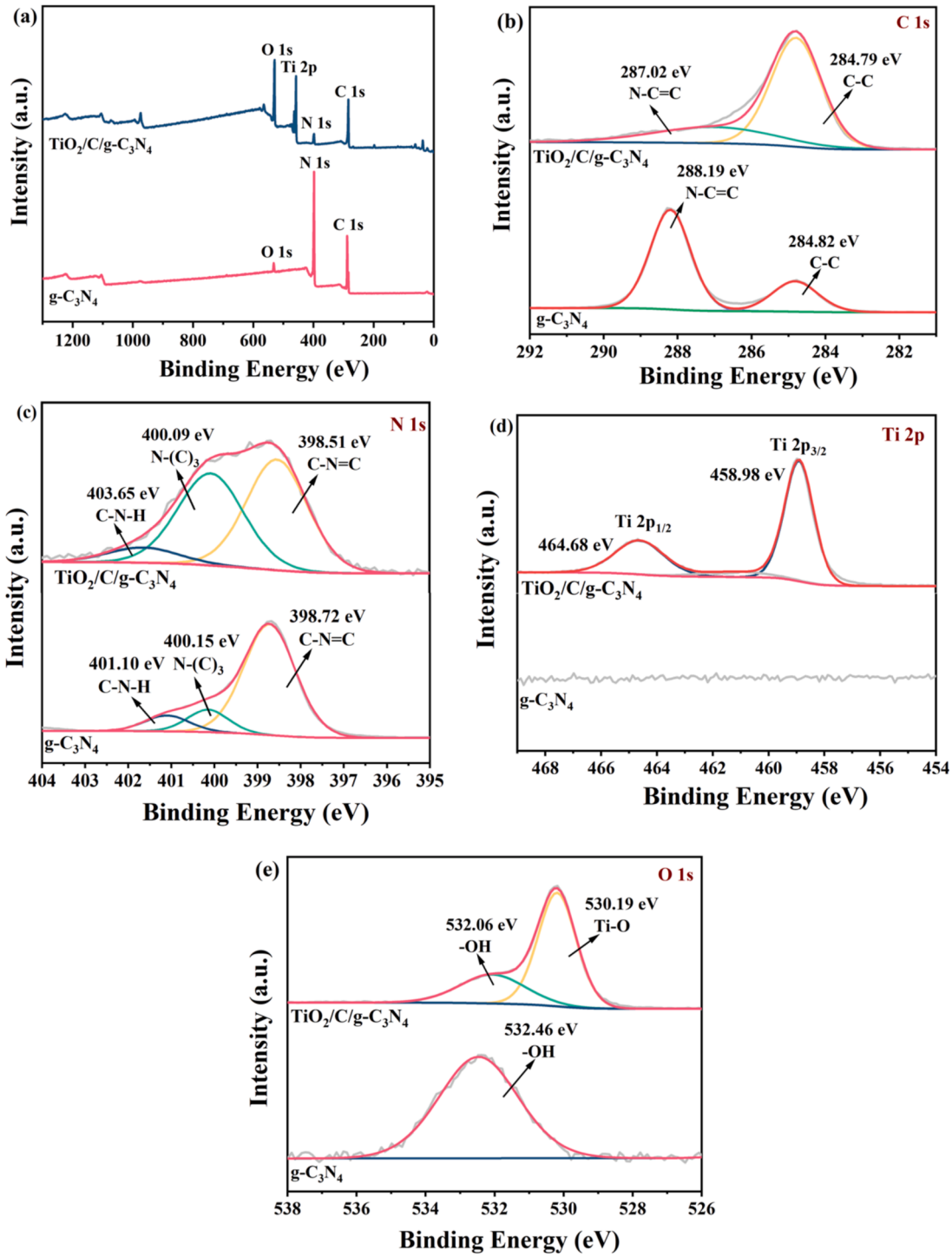

Fig. 3. XPS spectrum of (a) g-C_3N_4 and TiO_2/C/g-C_3N_4, XPS spectra with high resolution for C 1s (b), N 1s (c), Ti 2p (d), (e) O 1s for graphitic nitride (g-C_3N_4) and multi-junction (TiO_2/C/g-C_3N_4).

triazine molecules. Conversely, the minor peaks observed in the TiO_2/C/g-C_3N_4 hybrids within the range of 1200 to 1600 cm^{-1} are attributed to the typical N=C-N stretching mode inherent to heterocycles in g-C_3N_4. The broad band peaks between 3000 and 3500 cm^{-1} were attributed to N–H stretching vibration of the amine groups. These spectroscopic features collectively indicate effective coupling of g-C_3N_4 with the TiO_2/C/g-C_3N_4 hybrids (1, 2, 3). The strong bonding between g-C_3N_4 and the TiO_2/C/g-C_3N_4 hybrids (1, 2, 3) facilitates efficient charge transfer at the interface, resulting in enhanced photocatalytic activity. This bond promotes energetic electron transfer and generates synergistic interfacial effects, ultimately boosting the overall performance of the photocatalyst.

The X-ray photoelectron spectroscopy (XPS) was utilized to examine the different composition of the TiO_2/C/g-C_3N_4 hybrid photocatalysts. The energy band spectra were obtained using a C 1 s peak at (284.8 eV) for correcting the position of the peak. Fig. 3a-e shows the XPS analysis results for both pristine graphitic nitride and TiO_2/C/g-C_3N_4. The contents of C, N, Ti, and O components in the TiO_2/C/g-C_3N_4 hybrid sample are shown in Fig. 3a, indicating the integration of TiO_2 into g-C_3N_4. The C 1 s pattern of the TiO_2/C/g-C_3N_4 hybrid is displayed in Fig. 3b. The spectrum exhibits two distinct peaks related to carbon species. The strong peak in the higher energy range (287.2 eV to 288.19 eV) assigned to N-C=C bonding, while the second peak within the energy range (284.79 eV to 284.82 eV) represents C–C coordination, which is due to the presence of g-C_3N_4 (Wang et al., 2016). Fig. 3c demonstrates the high accuracy (N 1 s) spectra of TiO_2/C/g-C_3N_4 have peak in energy range (398.5 to 398.72) eV which assigned to C=N–C bond, while peaks in energy range (400.09–400.15) eV corresponds to N-(C3) bond (Wang et al., 2016) and the peaks appear in (401.10 eV 403.65 eV) energy range are designated to C–N–H bond (Wang et al., 2016; Li et al., 2014; Wang et al., 2023). In Fig. 3d, the Ti 2p spectrum has characteristic configurations, the sharpest of which are 464.68 eV is due to the Ti-$2p^{1/2}$ while 459 eV is assigned to Ti-$2p^{3/2}$ (Wang et al., 2023). The XPS results of (O 1s) are given Fig. 3e, which ascribed two peaks, 530.19 eV assigned to Ti-O bond and 532.46 eV to O–H bond (Jiang et al., 2018; Zou et al., 2017; Niu et al., 2012). The existence of a OH intermediates or water molecule upon that interface of the TiO_2/C/g-C_3N_4 hybrid structure is related to the presence of an O 1s peak at 532.06 eV. The XPS analysis demonstrates the effective formation of a heterostructure photocatalyst.

The catalytic activity of TiO_2/C/g-C_3N_4 hybrids in methyl orange (MO) degradation under visible light irradiation is depicted in Fig. 4a. When studying the performance of TiO_2/C/g-C_3N_4 hybrids catalyst, this research motivation is to combine the dual functions of chemical photocatalysis and physical adsorption. After physically adsorbing pollutants, there is a significant change of catalyst powders and MO solution in color. After absorption saturation, the color changed to light yellow due to MO (yellow) covering on catalyst. From Fig. 4a, it is true that the absorption of pollutants on catalyst surface is related to physical adsorption in dark. But it is NOT really degradation for MO pollutants based on the color-change observation. This process is mainly divided into two steps: physical adsorption and further chemical photo-degradation. In Fig. 4a the step-I explained the physical adsorption of MO onto catalyst surface in dark region mentioned in the corresponding Fig. 4a. The step-II confirmed the photocatalytic degradation of MO under light irradiation, which explained the photocatalytic properties. The results indicate a significant increase in MO adsorption capacity, with values rising from 18.0 % for g-C_3N_4 to 61.2 % for TiO_2/C/g-C_3N_4-1. Additionally, as the light-driven reaction proceeded, TiO_2/C/g-C_3N_4-1 hybrids exhibited a notable enhancement in the degradation rate of MO. Within a 180-minute period of visible light exposure, the MO photo-degradation efficiencies were measured as 93.6 %, 32.4 %, and

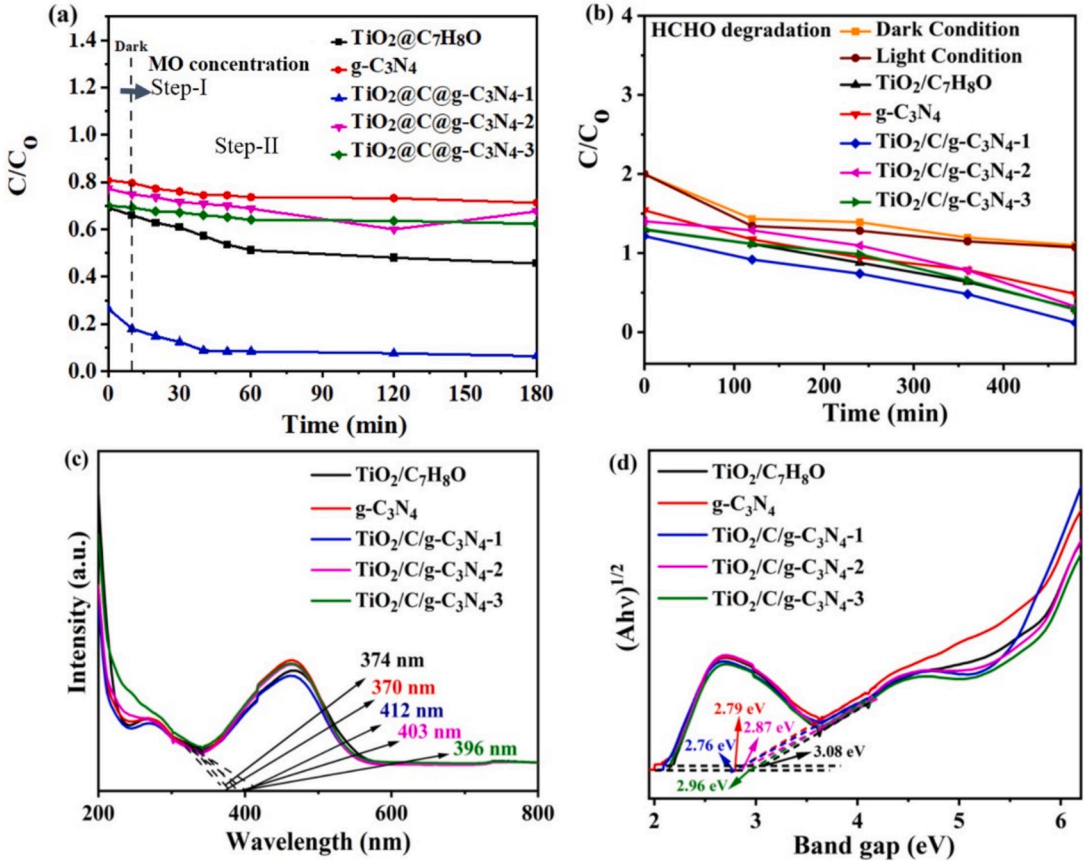

Fig. 4. Photocatalytic performance of (a) MO and (b) HCHO relative value MO concentration (C/C_0) of TiO_2/C hybrids. (c) UV–Vis absorbance spectra in the range of 200–800 nm and (d) Tauc plot by Kubelka-Munk equation of Pristine TiO_2/C_7H_8O, g-C_3N_4, TiO_2/C/g-C_3N_4-1, TiO_2/C/g-C_3N_4-2, TiO_2/C/g-C_3N_4-3.

37.6 % for TiO_2/C/g-C_3N_4-1, TiO_2/C/g-C_3N_4-2, and TiO_2/C/g-C_3N_4-3, respectively. Notably, TiO_2/C/g-C_3N_4-1 demonstrated superior photocatalytic degradation efficiency compared to the other two hybrids. This enhanced degradation capability was attributed to the presence of oxygen vacancies, defects, and primarily to the improved charge separation resulting from the hybridization between TiO_2, g-C_3N_4, and the carbon layer.

Furthermore, to assess the catalytic degradation activity, a photocatalytic device was utilized to evaluate the degradation of formaldehyde (HCHO) as a pollutant. The photocatalyst was applied onto cotton cloth, encapsulating HCHO within a closed chamber. The amount of HCHO evaporating from the chamber over a specified time period was monitored under LED illumination. These findings of this investigation are depicted in Fig. 4b. Notably, there was only a slight decrease in HCHO concentration within 8 h during the dark and blank experiments, likely attributed to HCHO evaporation through wiring pores. For TiO_2/C_7H_8O, the HCHO degradation rate after 8 h was only 42.2 %. However, the degradation rates of HCHO by TiO_2/C/g-C_3N_4-1 (93.7 %) exhibited significant improvement compared to TiO_2/C/g-C_3N_4-2 (83 %) and TiO_2/C/g-C_3N_4-3 (85 %). The formation of a hybrid incorporating an active carbon layer, type-II band alignment, and the introduction of oxygen vacancies contributes to the enhanced catalytic activity of TiO_2 materials within the visible light spectrum.

Using UV–Vis optical spectroscopy, energy gap values were estimated for TiO_2/C_7H_8O, TiO_2/C/g-C_3N_4-1, TiO_2/C/g-C_3N_4-2, and TiO_2/C/g-C_3N-3 hybrid materials. Notably, the TiO_2/C/g-C_3N_4-1 hybrids displayed absorption with a high-energy edge compared to TiO_2/C_7H_8O, indicating their superior ability to harness visible light. The absorption edges of TiO_2/C/g-C_3N_4-1, TiO_2/C/g-C_3N_4-2, and TiO_2/C/g-C_3N-3 were observed at 412 nm, 403 nm, and 396 nm, respectively, revealing clear red shifts in comparison to the 374 nm absorption edge of TiO_2/C_7H_8O. Remarkably, TiO_2/C/g-C_3N_4-1 exhibited a significant blue shift up to 412 nm.

The Tauc diagram, derived using the Kudelka-Munk formula Ahv1/2 = A(hv-Eg), provided insights into the bandgap energy (Eg) values. The Eg of TiO_2/C_7H_8O, g-C_3N_4, TiO_2/C/g-C_3N_4-1, TiO_2/C/g-C_3N_4-2, and TiO_2/C/g-C_3N_4-3 were determined as 3.08 eV, 2.79 eV, 2.76 eV, 2.87 eV, and 2.96 eV, respectively, as illustrated in Fig. 4d. Notably, TiO_2/C_7H_8O and TiO_2/C/g-C_3N_4-1 exhibited the lowest bandgap energies among the materials examined.

This observation correlates with the enhanced degradation efficiency for formaldehyde (HCHO), suggesting that the band structure of TiO_2/C_7H_8O is effectively tailored through doping materials to exploit the energy of visible light. This the importance of uniform carbon layer deposition on TiO_2 and the formation of novel hybrid structures, which effectively reduce the band gap of TiO_2. Ultimately, this modification positively impacts both physical adsorption and chemical degradation processes.

Furthermore, the study aimed to investigate the continuous cyclic degradation of organic dye pollutants, specifically HCHO and MO, in the presence of TiO_2/C/g-C_3N_4-1 under optical stimulation. The stability of TiO_2/C/g-C_3N_4-1 during the degradation process of MO and HCHO in light was examined, as shown in Fig. 5. It is found that the concentration of MO in the TiO_2/C cyclic degradation remained relatively stable after four cycles, indicating a consistent photo-degradation efficiency of approximately 93 %. This finding suggests that TiO_2/C/g-C_3N_4-1 maintained its high photocatalytic performance and stability throughout the cyclic degradation process, with no significant damage observed to the active sites on its surface. In Fig. 5b, it is observed that the degradation efficiency of TiO_2/C/g-C_3N_4-1 for HCHO gradually declined with each subsequent cycle, suggesting a reduction in its photocatalytic activity over time. This decline is attributed to

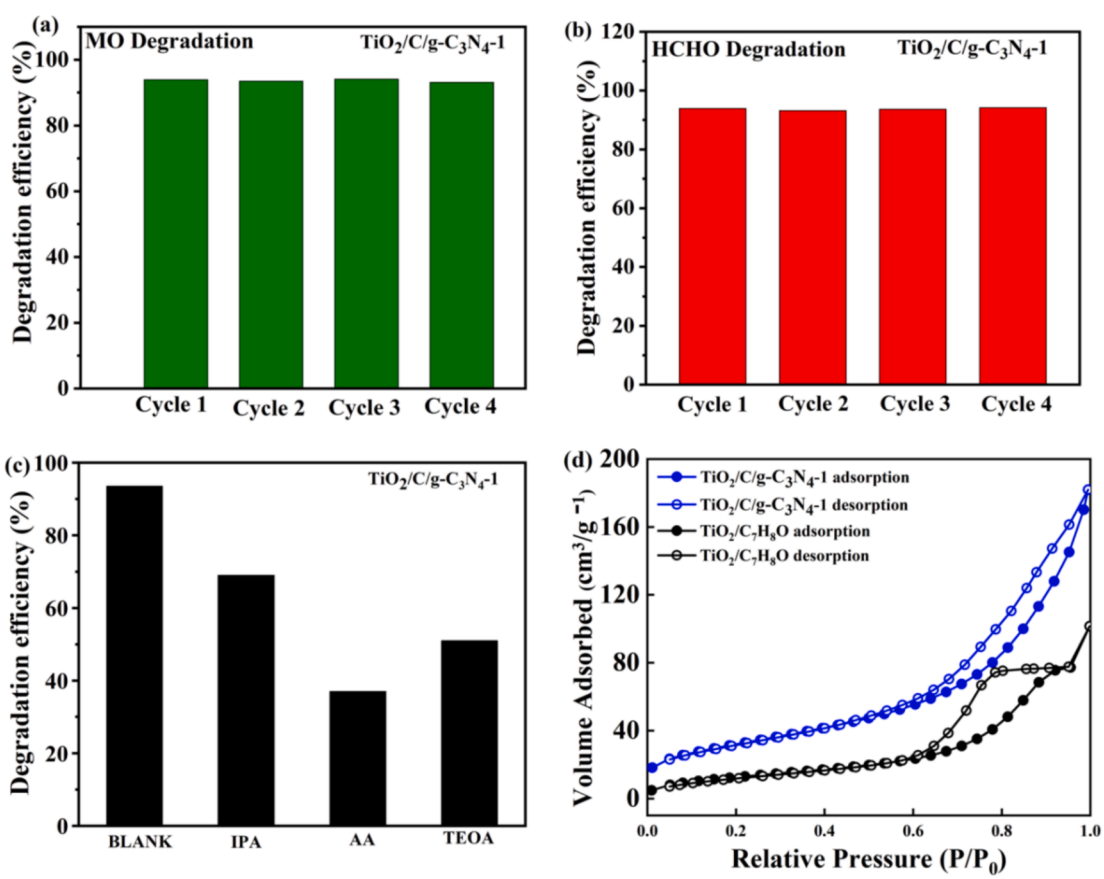

Fig. 5. Photocatalytic activity degradation cycle test of (a) HCHO and (b) MO by TiO_2/C/g-C_3N_4-1, (c) Photocatalytic degradation of MO by TiO_2/C/g-C_3N_4.1 with different scavengers under visible light, (d) N_2 adsorption/desorption isotherm TiO_2/C/g-C_3N_4 and TiO_2/C_7H_8O.

irreversible modifications on the surface state of $TiO_2/C/g\text{-}C_3N_4$ during the cyclic degradation of MO, leading to a gradual decrease in its photocatalytic performance. $TiO_2/C/g\text{-}C_3N_4$-1 exhibits remarkable activity and stability in the degradation of MO. Its surface, characterized by an amorphous structure and the presence of oxygen vacancy defects, facilitates efficient acceptance and transfer of photogenerated electrons (e^-) while inhibiting recombination with photogenerated holes (h^+). Several experiments were carried out to identify the active groups involved in the photodegradation process using MO as the target organic pollutant. The ascorbic acid (AA), triethanolamine (TEOA) and Isopropyl alcohol (IPA) were introduced as scavengers to capture $\cdot O_2-$, h^+, and *OH respectively. As shown in Fig. 5c, the addition of IPA had minimal impact on the degradation process, indicating that ·OH is not a major active species. However, the addition of AA significantly reduced degradation efficiency from 93.4 % (Blank sample) into 37.2 %, showing that O2·−, is the primary active species. When TEOA was added, the degradation efficiency decreased into 51.7 %, suggesting that h + is a secondary active species. In conclusion, O2·−, plays a major role while h + plays a minor role in the photocatalytic degradation of MO. The adsorption and desorption isotherms of N_2 were analyzed for $TiO_2/C/g\text{-}C_3N_4$ and TiO_2/C_7H_8O within a pressure range (0.0–1.0). The findings revealed that $TiO_2/C/g\text{-}C_3N_4$ exhibited a significantly higher specific surface area of approximately 181.2 m^2/g compared to TiO_2/C_7H_8O, which had a specific surface area of only about 100.96 m^2/g. This increased the specific surface area, creating more contact space between the $TiO_2/C/g\text{-}C_3N_4$ hybrid and the target pollutants. As a result, more active sites are available for efficient catalytic reactions.

The combination of dual functions of chemical photocatalysis and physical adsorption for $TiO_2/C/g\text{-}C_3N_4$ hybrid catalyst is developed. In terms of physical adsorption in dark, MO undergoes physical adsorption onto the hybrid catalyst surface, resulting in a slight darkening of the MO solution from dark yellow, reddish yellow into brown without degradation. The results highlight only physical adsorption it's not effective for MO degradation in dark. In terms of photocatalytic process, the schematic band alignment calculated using density functional theory (DFT) is shown in Fig. 6, highlighting the heterojunction between $g\text{-}C_3N_4$, carbon layer, and TiO_2, enabling effective charge transfer and separation of electrons and holes. Upon light irradiation, electrons are excited from the valence band (VB) to the conduction band (CB) of both $g\text{-}C_3N_4$ and TiO_2. The energy positions are crucial in directing charge carriers; $g\text{-}C_3N_4$'s CB at −1.16 eV and TiO_2's at −0.021 eV create a favorable pathway for electrons to migrate from $g\text{-}C_3N_4$ to TiO_2 via the carbon layer interface. Carbon layer acts as a conductive bridge, facilitating rapid electron transfer and minimizing electron-hole recombination. The carbon layer ensures the efficient transfer of electrons to the TiO_2 side for reduction reactions. Simultaneously, the holes generated in the valence band of $g\text{-}C_3N_4$ remain within the $g\text{-}C_3N_4$ layer, where they participate in oxidation reactions. This spatial separation of electrons and holes enhances the overall photocatalytic efficiency by reducing the likelihood of recombination. On the TiO_2 side, the electrons engage in the reduction of formaldehyde (HCHO), while on the $g\text{-}C_3N_4$ side, the holes are responsible for the oxidation of methyl orange (MO). The synergistic interaction between $g\text{-}C_3N_4$, carbon, and TiO_2 ensures that both oxidation and reduction reactions are occurring efficiently and in different zones. The alignment of the energy bands in this heterostructure enhances light absorption and charge transport, with the larger bandgap of TiO_2 (3.1 eV) enabling it to drive reduction reactions, while the narrower bandgap of $g\text{-}C_3N_4$ (1.49 eV) promotes hole-driven oxidation reactions. This arrangement ensures spatial separation of redox processes, significantly improving photocatalytic performance and pollutant degradation.

The advantage of $g\text{-}C_3N_4/C/TiO_2$ hybrid lies in their rapid physical adsorption of MO pollutants, which allows photocatalysts to degrade pollutants fast. This is due to the increased local concentration of pollutants on the catalyst surface. Besides, the $g\text{-}C_3N_4/C/TiO_2$ heterostructure's ability to absorb light energy efficiently, maintain charge separation, and optimize reaction zones makes it highly effective for the degradation of pollutants like MO and HCHO.

4. Conclusion

A novel hybrid photocatalyst of $TiO_2/C/g\text{-}C_3N_4$ is developed through an efficient air calcination technique and precursory methodology. This hybrid photocatalyst demonstrates remarkable efficacy in catalyzing the degradation of organic compounds and air pollutants. Notably, among the synthesized samples, the $g\text{-}C_3N_4/C/TiO_2$ hybrid photocatalyst exhibits that the catalyst efficiently adsorbs MO in dark without degradation. Combining physical adsorption with photocatalytic activity, it

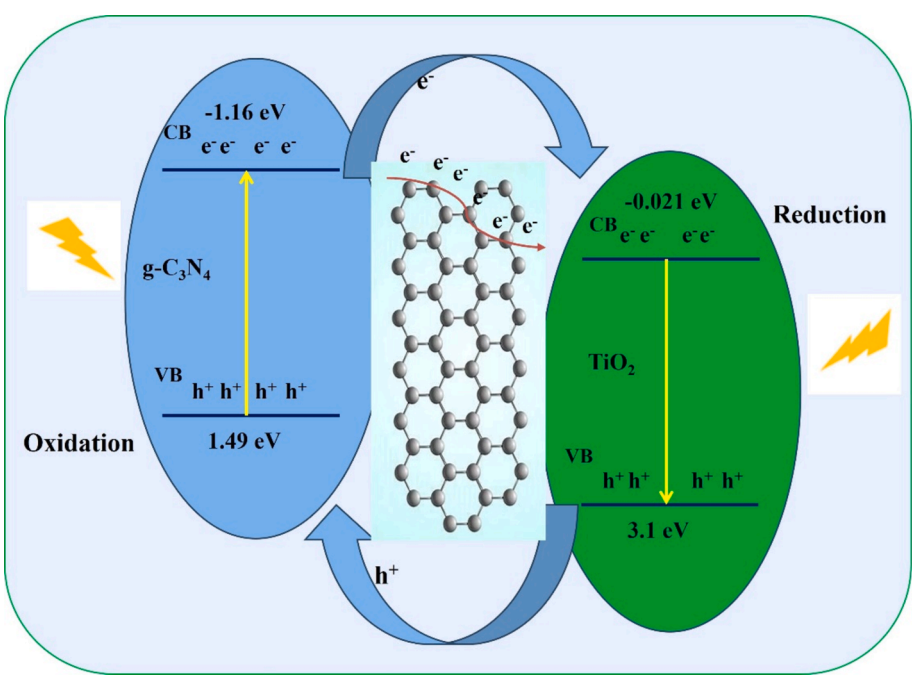

Fig. 6. The staggered band alignment and charge carrier separation in $TiO_2/C/g\text{-}C_3N_4$ composite structures.

degrades 94 % of MO and HCHO within 180 min at an initial concentration of 0.2 mol/L, achieving almost complete decolorization under visible light irradiation. The observed enhancement in catalytic performance is attributed to the staggered band alignment within the TiO_2/C/g-C_3N_4 hybrid photocatalyst, facilitating efficient charge separation and promoting electron transfer at the interface, thereby accelerating catalytic reactions. Furthermore, the incorporation of carbon layers speeds up electron transport, contributing to the enhanced degradation of MO and HCHO within the TiO_2/C/g-C_3N_4 hybrid photocatalyst. This study introduces a straightforward and cost-effective approach for fabricating hybrid TiO_2/C/g-C_3N_4 photocatalysts, with potential scalability for the practical applications.

CRediT authorship contribution statement

Azim Khan: Writing – review & editing, Writing – original draft, Data curation, Conceptualization. **Ruhumuriza Jonathan:** Writing – original draft, Methodology, Data curation. **Shafiq Ur Rehman:** Writing – review & editing, Data curation. **Muhammad Shoaib:** Writing – review & editing, Data curation. **Feng Cao:** Writing – review & editing, Investigation, Data curation. **Sajjad Ali:** Writing – review & editing, Data curation, Conceptualization. **Mohamed Bououdina:** Writing – review & editing, Data curation, Conceptualization. **Pir Muhammad Ismail:** Writing – review & editing, Investigation, Formal analysis. **Junwei Wang:** Writing – review & editing, Formal analysis, Data curation, Conceptualization. **Hazem Abu-Farsakh:** Writing – review & editing, Funding acquisition, Formal analysis, Data curation. **Yifan Liu:** Writing – review & editing, Formal analysis, Data curation. **Xian Jian:** Supervision, Project administration, Funding acquisition, Formal analysis, Conceptualization.

Declaration of Competing Interest

The authors declare that they have no known competing financial interests or personal relationships that could have appeared to influence the work reported in this paper.

Acknowledgements

The financial supported in this work was provided by National Natural Science Foundation of China (No. 51972045), Sichuan Science and Technology Program (Nos. 2022NSFSC1087, 2021YFG0373). The author would like to thank Prince Sultan University for their support.

References

Bao, L., Ren, X., Liu, C., Liu, X., Dai, C., Yang, Y., Bououdina, M., Ali, S., Zeng, C., 2023. Modulating the doping state of transition metal ions in ZnS for enhanced photocatalytic activity. Chem. Commun. 59, 11280–11283. https://doi.org/10.1039/d3cc03436d.

Bashir, M., Majid, F., Bibi, I., Mushtaq, J., Ali, A., Farhat, L.B., Katubi, K.M., Alwadai, N., Khan, M.I., Iqbal, M., 2022. Ultrasonic assisted synthesis of ZnO nanoflakes and photocatalytic activity evaluation for the degradation of methyl orange. Arab. J. Chem. 15. https://doi.org/10.1016/j.arabjc.2022.104194.

Cao, S.W., Yuan, Y.P., Fang, J., Shahjamali, M.M., Boey, F.Y.C., Barber, J., Joachim Loo, S.C., Xue, C., 2013. In-situ growth of CdS quantum dots on g-C3N4 nanosheets for highly efficient photocatalytic hydrogen generation under visible light irradiation. Int. J. Hydrogen Energy 38, 1258–1266. https://doi.org/10.1016/j.ijhydene.2012.10.116.

Chen, Y., Wang, Y., Li, W., Yang, Q., Hou, Q., Wei, L., Liu, L., Huang, F., Ju, M., 2017. Enhancement of photocatalytic performance with the use of noble-metal-decorated TiO2 nanocrystals as highly active catalysts for aerobic oxidation under visible-light irradiation. Appl. Catal. B Environ. 210, 352–367. https://doi.org/10.1016/j.apcatb.2017.03.077.

Chen, H., Xing, Y., Liu, S., Liang, Y., Fu, J., Wang, L., Wang, W., 2023. Mechanistic insights into efficient photocatalytic H2O2 production of 2D/2D g-C3N4/In2S3 photocatalyst by tracking charge flow direction. Chem. Eng. J. 462. https://doi.org/10.1016/j.cej.2023.142038.

Cui, Y., 2006. Photocatalytic degradation of MO by complex nanometer particles WO3/TiO2. Rare Met. 25, 649–653. https://doi.org/10.1016/S1001-0521(07)60007-2.

Cui, Y., Sun, W., 2006. Degradation of BPB in photocatalysis enhanced by photosensitizer. Rare Met. 25, 138–143. https://doi.org/10.1016/S1001-0521(06)60029-6.

Dalanta, F., Kusworo, T.D., Aryanti, N., 2022. Synthesis, characterization, and performance evaluation of UV light-driven Co-TiO2@SiO2 based photocatalytic nanohybrid polysulfone membrane for effective treatment of petroleum refinery wastewater. Appl. Catal. B Environ. 316. https://doi.org/10.1016/j.apcatb.2022.121576.

Djurišić, A.B., Leung, Y.H., Ching Ng, A.M., 2014. Strategies for improving the efficiency of semiconductor metal oxide photocatalysis. Horizons Mater. https://doi.org/10.1039/c4mh00031e.

Guo, Z., Wu, H., Li, M., Tang, T., Wen, J., Li, X., 2020. Phosphorus-doped graphene quantum dots loaded on TiO2 for enhanced photodegradation. Appl. Surf. Sci. 526. https://doi.org/10.1016/j.apsusc.2020.146724.

Guo, Z., Ni, S., Wu, H., Wen, J., Li, X., Tang, T., Li, M., Liu, M., 2021. Designing nitrogen and phosphorus co-doped graphene quantum dots/g-C3N4 heterojunction composites to enhance visible and ultraviolet photocatalytic activity. Appl. Surf. Sci. 548. https://doi.org/10.1016/j.apsusc.2021.149211.

Han, C., Cheng, C., Liu, F., Li, X., Wang, G., Li, J., 2023. Preparation of CdS-Ag2S nanocomposites by ultrasound-assisted UV photolysis treatment and its visible light photocatalysis activity. Nanotechnol. Rev. 12. https://doi.org/10.1515/ntrev-2022-0503.

Huang, Z., Jia, S., Wei, J., Shao, Z., 2021. A visible light active, carbon-nitrogen-sulfur co-doped TiO2/g-C3N4Z-scheme heterojunction as an effective photocatalyst to remove dye pollutants. RSC Adv. 11, 16747–16754. https://doi.org/10.1039/d1ra01890f.

Inoue, T., Fujishima, A., Konishi, S., Honda, K., 1979. Photoelectrocatalytic reduction of carbon dioxide in aqueous suspensions of semiconductor powders [3]. Nature. https://doi.org/10.1038/277637a0.

Ismael, M., 2020. A review on graphitic carbon nitride (g-C3N4) based nanocomposites: Synthesis, categories, and their application in photocatalysis. J. Alloy. Compd. https://doi.org/10.1016/j.jallcom.2020.156446.

Jiang, X.H., Xing, Q.J., Luo, X.B., Li, F., Zou, J.P., Liu, S.S., Li, X., Wang, X.K., 2018. Simultaneous photoreduction of Uranium(VI) and photooxidation of Arsenic(III) in aqueous solution over g-C3N4/TiO2 heterostructured catalysts under simulated sunlight irradiation. Appl. Catal. B Environ. 228, 29–38. https://doi.org/10.1016/j.apcatb.2018.01.062.

Jiao, W., Zhang, L., Yang, R., Ning, J., Xiao, L., Liu, Y., Ma, J., Mahmood, N., Jian, X., 2022. Synthesis of monolayer carbon-coated TiO2 as visible-light-responsive photocatalysts. Appl. Mater. Today 27. https://doi.org/10.1016/j.apmt.2022.101498.

Jonathan, R., Ur Rehman, S., Cao, F., Xu, H., Ma, X., Wang, J., Liu, Y., Niu, Y., Jian, X., Mahmood, N., 2023. Low-cost and large-scale preparation of ultrafine TiO2@C hybrids for high-performance degradation of methyl orange and formaldehyde under visible light. Nanotechnol. Rev. 12. https://doi.org/10.1515/ntrev-2022-0556.

Li, X., Fang, G., Qian, X., Tian, Q., 2022. Z-scheme heterojunction of low conduction band potential MnO2 and biochar-based g-C3N4 for efficient formaldehyde degradation. Chem. Eng. J. 428. https://doi.org/10.1016/j.cej.2021.131052.

Li, H., Liu, J., Hou, W., Du, N., Zhang, R., Tao, X., 2014. Synthesis and characterization of g-C3N4/Bi2MoO6 heterojunctions with enhanced visible light photocatalytic activity. Appl. Catal. B Environ. 160–161, 89–97. https://doi.org/10.1016/j.apcatb.2014.05.019.

Lin, Y., Zhang, Q., Li, Y., Liu, Y., Xu, K., Huang, J., Zhou, X., Peng, F., 2020. The Evolution from a Typical Type-I CdS/ZnS to Type-II and Z-Scheme Hybrid Structure for Efficient and Stable Hydrogen Production under Visible Light. ACS Sustain. Chem. Eng. 8, 4537–4546. https://doi.org/10.1021/acssuschemeng.0c00101.

Liyanaarachchi, H., Thambiliyagodage, C., Liyanaarachchi, C., Samarakoon, U., 2023. Efficient photocatalysis of Cu doped TiO2/g-C3N4 for the photodegradation of methylene blue. Arab. J. Chem. 16. https://doi.org/10.1016/j.arabjc.2023.104749.

Lu, X., Wang, Q., Cui, D., 2010. Preparation and Photocatalytic Properties of g-C3N4/TiO2 Hybrid Composite. J. Mater. Sci. Technol. 26, 925–930. https://doi.org/10.1016/S1005-0302(10)60149-1.

Luo, J., Chen, J., Guo, R., Qiu, Y., Li, W., Zhou, X., Ning, X., Zhan, L., 2019. Rational construction of direct Z-scheme LaMnO3/g-C3N4 hybrid for improved visible-light photocatalytic tetracycline degradation. Sep. Purif. Technol. 211, 882–894. https://doi.org/10.1016/j.seppur.2018.10.062.

Luo, J., Ning, X., Zhan, L., Zhou, X., 2021. Facile construction of a fascinating Z-scheme AgI/Zn3V2O8 photocatalyst for the photocatalytic degradation of tetracycline under visible light irradiation. Sep. Purif. Technol. 255. https://doi.org/10.1016/j.seppur.2020.117691.

Nguyen, V.H., Smith, S.M., Wantala, K., Kajitvichyanukul, P., 2020. Photocatalytic remediation of persistent organic pollutants (POPs): A review. Arab. J. Chem. https://doi.org/10.1016/j.arabjc.2020.04.028.

Niu, P., Liu, G., Cheng, H.M., 2012. Nitrogen vacancy-promoted photocatalytic activity of graphitic carbon nitride. J. Phys. Chem. C 116, 11013–11018. https://doi.org/10.1021/jp301026y.

Osterloh, F.E., 2013. Inorganic nanostructures for photoelectrochemical and photocatalytic water splitting. Chem. Soc. Rev. 42, 2294–2320. https://doi.org/10.1039/c2cs35266d.

Que, M., Cai, W., Chen, J., Zhu, L., Yang, Y., 2021. Recent advances in g-C3N4composites within four types of heterojunctions for photocatalytic CO2reduction. Nanoscale. https://doi.org/10.1039/d0nr09177d.

Shaban, Y.A., 2019. Solar light-induced photodegradation of chrysene in seawater in the presence of carbon-modified n-TiO2 nanoparticles. Arab. J. Chem. 12, 652–663. https://doi.org/10.1016/j.arabjc.2018.01.007.

Shi, J., Jiang, J., Chen, Q., Wang, L., Nian, K., Long, T., 2023. Production of higher toxic intermediates of organic pollutants during chemical oxidation processes: A review. Arab. J. Chem. https://doi.org/10.1016/j.arabjc.2023.104856.

Sun, S., Ding, H., Mei, L., Chen, Y., Hao, Q., Chen, W., Xu, Z., Chen, D., 2020. Construction of SiO2-TiO2/g-C3N4 composite photocatalyst for hydrogen production and pollutant degradation: Insight into the effect of SiO2. Chinese Chem. Lett. 31, 2287–2294. https://doi.org/10.1016/j.cclet.2020.03.026.

Wang, K., Huang, D., Li, X., Feng, K., Shao, M., Yi, J., He, W., Qiao, L., 2023. Unconventional strategies to break through the efficiency of light-driven water splitting: A review. Electron 1. https://doi.org/10.1002/elt2.4.

Wang, J., Wang, S., 2022. A critical review on graphitic carbon nitride (g-C3N4)-based materials: Preparation, modification and environmental application. Coord. Chem. Rev. https://doi.org/10.1016/j.ccr.2021.214338.

Wang, Y., Xu, Y., Wang, Y., Qin, H., Li, X., Zuo, Y., Kang, S., Cui, L., 2016. Synthesis of Mo-doped graphitic carbon nitride catalysts and their photocatalytic activity in the reduction of CO2 with H2O. Catal. Commun. 74, 75–79. https://doi.org/10.1016/j.catcom.2015.10.029.

Wang, H.Y., Yang, Y., Li, X., Li, L.J., Wang, C., 2010. Preparation and characterization of porous TiO2/ZnO composite nanofibers via electrospinning. Chinese Chem. Lett. 21, 1119–1123. https://doi.org/10.1016/j.cclet.2010.03.009.

Wang, Y., Yu, J., Peng, W., Tian, J., Yang, C., 2019. Novel multilayer TiO2 heterojunction decorated by low g-C3N4 content and its enhanced photocatalytic activity under UV, visible and solar light irradiation. Sci. Rep. 9. https://doi.org/10.1038/s41598-019-42438-w.

Wu, L., Li, Y., Zhou, B., Liu, J., Cheng, D., Guo, S., Xu, K., Yuan, C., Wang, M., Hong Melvin, G.J., Ortiz-Medina, J., Ali, S., Yang, T., Kim, Y.A., Wang, Z., 2023. Vertical graphene on rice-husk-derived SiC/C composite for highly selective photocatalytic CO2 reduction into CO. Carbon N. Y. 207, 36–48. https://doi.org/10.1016/j.carbon.2023.03.003.

Wudil, Y.S., Ahmad, U.F., Gondal, M.A., Al-Osta, M.A., Almohammedi, A., Sa'id, R.S., Hrahsheh, F., Haruna, K., Mohamed, M.J.S., 2023. Tuning of graphitic carbon nitride (g-C3N4) for photocatalysis: A critical review. Arab. J. Chem. https://doi.org/10.1016/j.arabjc.2023.104542.

Xiao, C., Leow, W.R., Chen, L., Li, Y., Li, C., 2023. Electrocatalytic conversion of waste polyamide-66 hydrolysates into high-added-value adiponitrile and hydrogen fuel. Electron 1. https://doi.org/10.1002/elt2.14.

Xin, Z., Zhao, X., Ji, H., Ma, T., Li, H., Zhong, S., Shen, Z., 2021. Amorphous carbon-linked TiO2/carbon nanotube film composite with enhanced photocatalytic performance: The effect of interface contact and hydrophilicity. Chinese Chem. Lett. 32, 2151–2154. https://doi.org/10.1016/j.cclet.2020.11.054.

Xu, R., Wei, G., Xie, Z., Diao, S., Wen, J., Tang, T., Jiang, L., Li, M., Hu, G., 2024. V2C MXene–modified g-C3N4 for enhanced visible-light photocatalytic activity. J. Alloy. Compd. 970. https://doi.org/10.1016/j.jallcom.2023.172656.

Yan, Y., Wang, H., Bi, X., Zhao, Y., Wang, W., Wu, M., 2023. Tandem catalysts CuSe/Au X for increasing local *CO concentration to promote the photocatalytic CO 2 reduction to C_2H_4. Electron 1. https://doi.org/10.1002/elt2.3.

Yao, S., Ma, Y., Xu, T., Wang, Z., Lv, P., Zheng, J., Ma, C., Yu, K., Wei, W., Ostrikov, K. (Ken), 2021. Ti–C bonds reinforced TiO2@C nanocomposite Na-ion battery electrodes by fluidized-bed plasma-enhanced chemical vapor deposition. Carbon N. Y. 171, 524–531. https://doi.org/10.1016/j.carbon.2020.09.023.

Yin, Y., Wang, J., Chen, B., Zhang, P., Li, G., Sun, W., Hu, F.X., Li, C.M., 2022. Unique BiFeO3/g-C3N4mushroom heterojunction with photocatalytic antibacterial and wound therapeutic activity. Nanoscale 14, 2686–2695. https://doi.org/10.1039/d1nr08016d.

Zhang, W., Hou, J., Bai, M., He, C., Wen, J., 2023. Spontaneously enhanced visible-light-driven photocatalytic water splitting of type II PG/AlAs5 van der Waal heterostructure: A first-principles study. Chinese Chem. Lett. 34. https://doi.org/10.1016/j.cclet.2023.108270.

Zou, Y., Shi, J.W., Ma, D., Fan, Z., Lu, L., Niu, C., 2017. In situ synthesis of C-doped TiO2@g-C3N4 core-shell hollow nanospheres with enhanced visible-light photocatalytic activity for H2 evolution. Chem. Eng. J. 322, 435–444. https://doi.org/10.1016/j.cej.2017.04.056.